XMM-Newton CCF Release Note

XMM-SOC-CAL-SRN-0306

Calibration of the Rate-Dependent PHA (RDPHA) correction for EPIC-pn Timing Mode

M. Guainazzi

October 1, 2013

1 CCF components

Name of CCF	VALDATE	EVALDATE	Blocks changed	XSCS flag
EPN_CTI_0030.CCF	2001-01-01		RDPHA_DERIV	NO

2 The need for this calibration update

The energy scale in EPIC-pn Timing Mode is affected by two effects, that are not significant in imaging modes: X-ray Loading (XRL; Smith 2004), and a count rate dependence (Sala et al. 2008). The latter effect has been traditionally attributed to a rate-dependent Charge Transfer Inefficiency (CTI; Guainazzi et al. 2008). However, its origin is still uncertain.

Guainazzi (2013) describes a new scheme to correct for the energy scale rate dependence in EPIC-pn Timing Mode exposures. This correction was christened **"Rate-Dependent PHA"** (RDPHA). In this scheme, the energy scale is calibrated by fitting the peaks in derivative PHA spectra corresponding to the Si ($\simeq$1.7 keV) and Au ($\simeq$2.3 keV) edges of the instrumental response, where the gradient of the effective area is the largest. Guainazzi (2013) suggests that this scheme is superior to the Rate-Dependent CTI (RDCTI) scheme currently implemented in the SAS through the standalone task `epfast`, because: a) it is independent on any assumptions on the astrophysical model in the spectral region around the edges; b) it is calibrated in PHA space, before events are corrected for gain and CTI. The latter avoids circularity in the calibration process.

The scientific validation of the CCF version described in Guainazzi (2013) (`EPN_CTI_0027.CCF`) unveiled that the underlying calibration function was insufficient. It has been therefore decided to postpone the public release of this calibration method, awaiting for a more accurate and flexible implementation scheme in the SAS. The CCF described in this Release Note implements this new scheme.

3 Changes

The main changes between EPN_CTI_0027.CCF (Guainazzi 2013) and EPN_CTI_0030.CCF (this document) are: a) the analytical function used to fit the calibration data; b) the new format of the calibration file extension.

3.1 Fit of calibration data

In Guainazzi (2013) the RDPHA calibration data were fit with a simple linear function:

$$\Delta PHA^{CCF27} \propto N_e$$

where ΔPHA^{CCF27} was the energy scale shift induced by a total (source+background) count rate expressed in units of the number of shifted electrons during the observation (N_e; see Guainazzi et al. 2013a, for a definition of this quantity, and a discussion of the rationale behind its usage). This function is insufficient to describe the RDPHA correction for sources with low count rates. The calibration embedded in the new CCF is based on fitting the same calibration data as in Guainazzi (2013) with a double power-law function:

$$PHA = A_1 \quad \text{for } N_e \leq N_e^{th}$$

$$PHA = A_2 + A_3 \times \log(N_e) \quad \text{for } N_e > N_e^{th}$$

whose fit parameters are A_1, A_3 and N_e^{th}, and A_2 is determined by the condition of continuity at N_e^{th}. Data points corresponding to the Si and Au edges were fit independently (Fig. 1). The CCF contains the values $\Delta PHA \equiv PHA(N_e) - PHA(0)$. The SAS combines the fit results at the Si and Au edges to determine the correction for each observation, weighting them by the statistical errors propagated from the uncertainties on the fit parameters.

3.2 CCF tabular structure

In EPN_CTI_0027.CCF the RDPHA correction was described through the coefficients of the ΔPHA^{CCF27} versus N_e linear fit. While conceptually cleaner, this solution implies that a change in the SAS is required whenever the fitting function changes. As of EPN_CTI_0030.CCF, the calibrated values of ΔPHA (together with their statistical uncertainties) are tabulated on a logarithmically equispaced grid of 100 N_e values in the range 10 to 2500. Any future changes or evolution of the calibration function *will not require a change in the CAL and/or in* `epevents`.

4 Scientific Impact of this Update

This CCF is the third calibration update driven by the recent discovery of ubiquitous XRL in the spectra of EPIC-pn Timing Mode exposures. The previous calibration updates

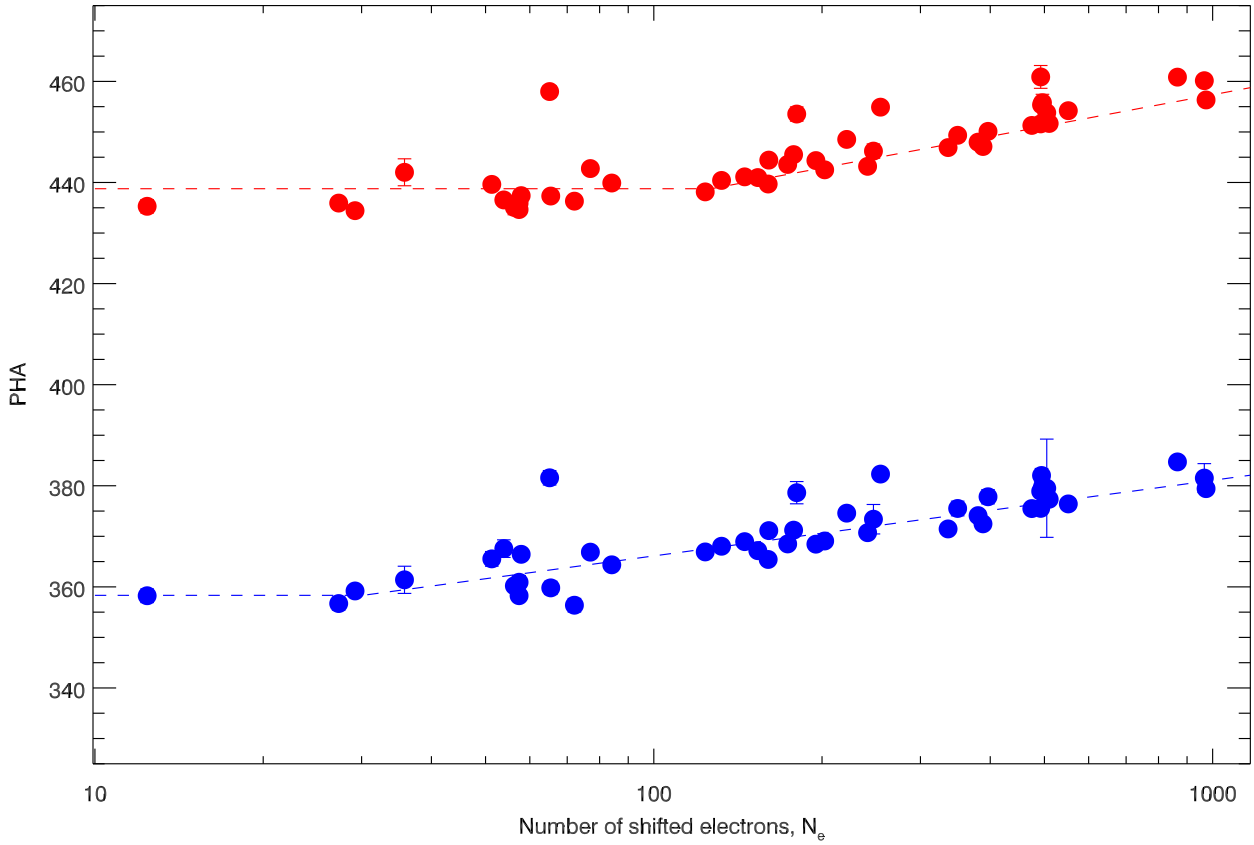

Figure 1: Calibration of the RDPHA correction at the Si (*red*) and Au (*blue*) edges. The *dashed lines* represent the best-fit broken power-law models to the data.

implemented the XRL correction (Guainazzi et al. 2013b) and the associated recalibration of the RDCTI (Guainazzi 2013b).

The RDPHA is intended to improve the homogeneity of the energy reconstruction accuracy over the wide range of count rates that sources observed in EPIC-pn Timing Mode exhibit. This is particularly critical for sources with count rates larger then a few hundreds counts per second, for which the rate-dependent effect shows a steeper gradient with N_e.

Sources with a total (source+background) count rate larger then $\simeq$800 counts per second are affected by pile-up in EPIC-pn Timing Mode. This threshold can be lower by as much as a factor of two for very steep, or very flat sources (see the discussion in the XMM-Newton User's Handbook, Longinotti et al. 2013). Neither the RDCTI nor the RDPHA correction are intended or expected to correct the energy distortions induced by pile-up.

4.1 Why using the RDPHA instead of the RDCTI?

In principle both the RDPHA (applied through the parameter `withrdpha` in `epevents`) and the RDCTI correction (applied through the standalone SAS task `epfast`) are intended to account and correct for the dependence of the energy scale on the total (source+background) count rate (hence the "RD" string in their name). For reasons described in Sect. 2, the RDPHA correction is expected to yield a better energy scale accuracy than the RDCTI correction.

In SAS versions later than 13 both corrections are available. We recommend users to try and use them, and compare their results. Feedback to the XMM-Newton Science Operations Centre HelpDesk (available at: `http://xmm.esac.esa.int/external/xmm_user_support/helpdesk.shtml`) are welcome.

5 Estimated Scientific Quality

The RDPHA correction is intended to eventually replace the RDCTI correction. The goal of the RDPHA correction is achieving an accuracy of energy scale reconstruction around 2 keV within ±20 eV.

The RDPHA correction is applied by `epevents` through the parameter `withrdpha`. It is *not applied by default* in SASv13.0: users must set explicitly `withrdpha=yes`.

The RDPHA and RDCTI corrections are mutually exclusive. Applying both on the same data-sets would yield an erroneous energy scale. This is in principle impossible: `epfast` does not apply the RDCTI correction on an event list, on which the RDPHA correction was applied, and issues a warning.

5.1 Accuracy of the energy reconstruction at the instrumental edges

Fig. 2 shows an histogram of the difference δE between the measured and modelled ΔPHA for the objects used for the calibration of the RDPHA (cf. Fig. 1).[1] The standard deviation is ≃20 eV at both the Si and the Au energies. The slightly larger-than-zero median of the distribution is consistent with the typical systematic uncertainties of the EPIC-pn gain during an observation.

[1]We use here the standard conversion factor between energy and PHA channel: 1 ADU = 5 eV. However, users shall remember that the RDPHA correction is calibrated in PHA space. The abscissa scale in the histograms in Fig. 1 is therefore only approximate, because it does not take into account gain non-linearity and/or redistribution effects.

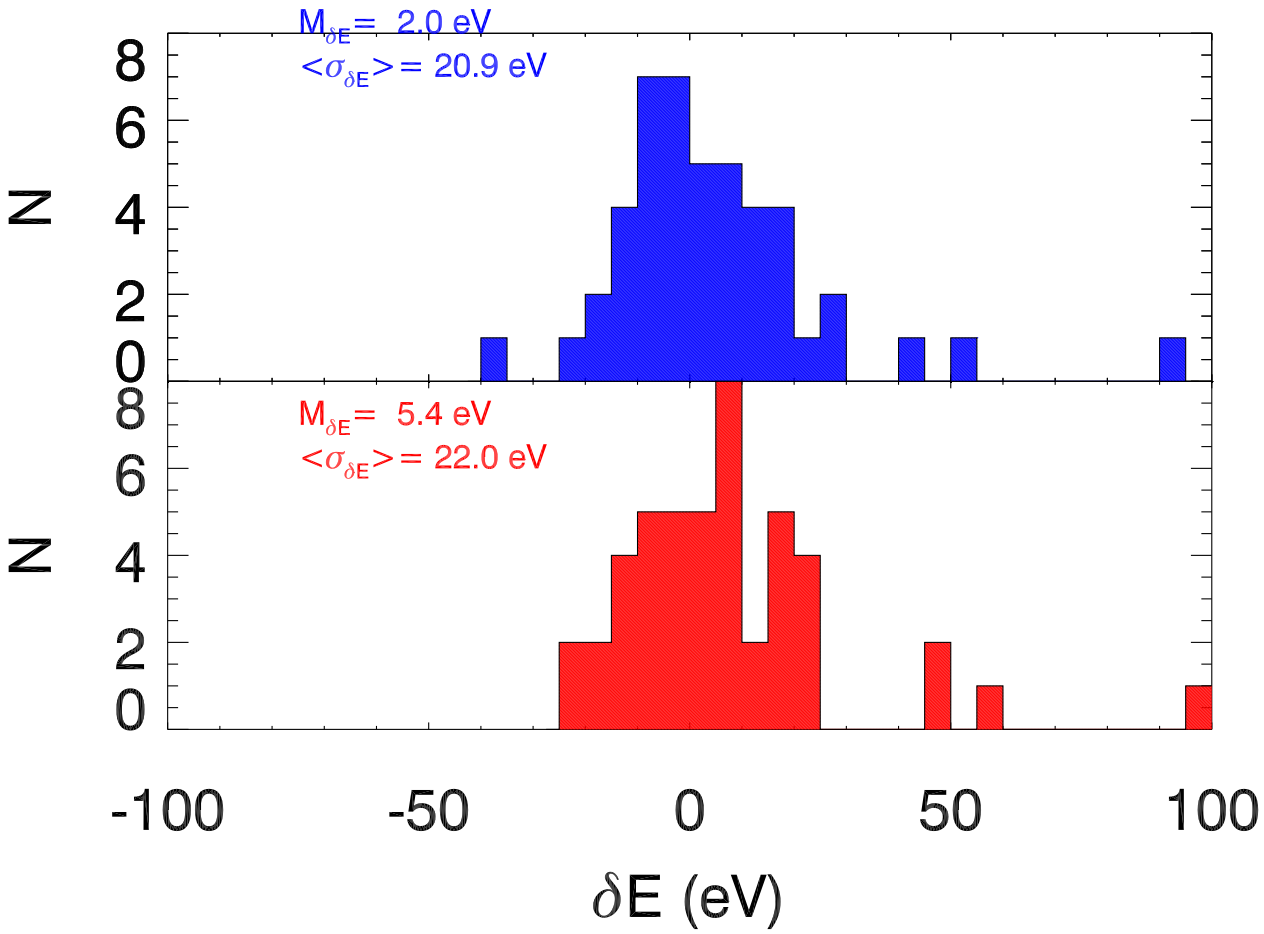

Figure 2: Distribution of the energy scale accuracy (in eV) at the energies of the Si (*upper panel*) and Au (*lower panel*) edges, following the application of the RDPHA correction to the sample used for the correction global calibration.

5.2 Accuracy of the energy reconstruction at the Fe energies

While the calibration at the Si and Au edges made use of a large number of well-exposed spectra, the scientific validation at higher and lower energies is limited by the small number of sources where independent observables of the energy scales are available. This is particularly crucial around 6 keV.

A first assessment of the quality of the energy reconstruction at the energies of Fe fluorescence and recombination transitions was made using four observations of celestial sources, exhibiting prominent narrow-band features above 6 keV. The energy scale yielded by the RDPHA is consistent with the atomic physics predictions for observations corresponding to N_e $\leq$100: XB 1323-619 (Obs.#0036140201), 4U1915-05 (Obs.#0085290301), RS Oph (Obs.#0410180101). The performances were worse for the source with the highest count rate, GX13+1 (Obs.#0122340901). This bright (net count rate in the 0.7–10 keV energy band $\geq$400 s^{-1}) source exhibits prominent absorption lines due to resonant transitions of highly ionised iron. I discuss this discrepant case in more details in the next paragraph

Calibrated event lists were reduced applying the XRL correction only, whence the spectra shown in Fig. 3 were extracted. I extracted four spectra corresponding to the boresight

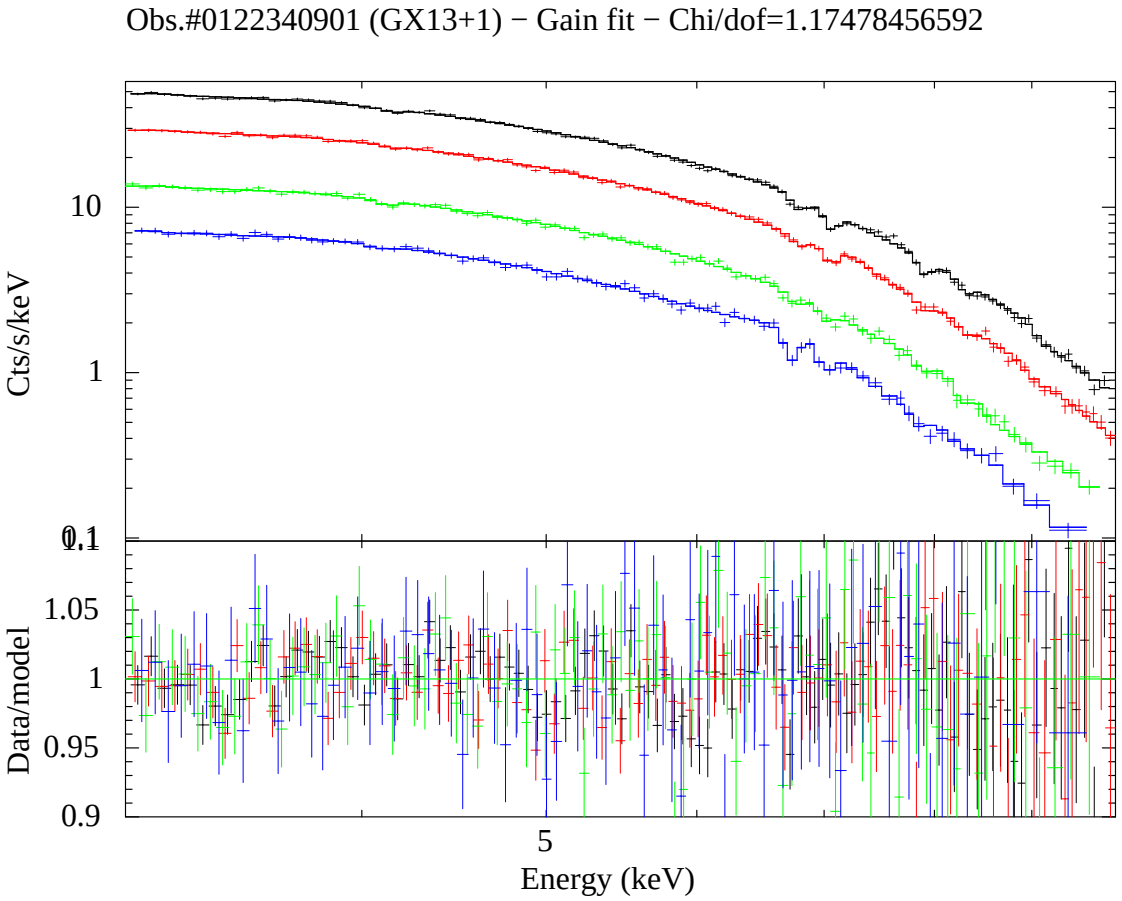

Figure 3: Spectrum of GX13+1 (Obs.#0122340901; *upper panel*) and residuals against the best-fit model (*lower panel*; details in text) when a constant offset of the energy scale is applied. The `PHA` column in the event list was corrected for XRL only. The additional shift required to adjust the energy scale to match the laboratory energies of the resonant transitions of FeXXV and FeXXVI exceeds that calibrated at the Si and Au instrumental edges by ≃20 eV for the three "off-axis" spectra, by ≃40 eV for the boresight spectrum.

column, and to three adjacent columns ("off-axis columns" hereafter). The spectra were fit simultaneously with the same astrophysical model, constituted by a standard X-ray binary continuum (multicolour disk black-body plus power-law), and two absorption lines corresponding to resonant absorption by FeXXV, and FeXXVI, plus three additional absorption lines at higher energies, on whose nature no assumption was made, and whose centroid energies was left free to vary (the best-fit values are ≃7.8, 8.2[2], and 9.5 keV, respectively). The RDPHA calibrated at the Si and Au instrumental edges over-corrects the energy scale at the Fe line energies by ≃20 eV for the 3 off-axis spectra. The error is larger for the boresight spectrum, suggesting a possible flattening of the RDPHA at high count rates.

The proposed CCF includes an independent column for the correction at (the `PHA` value

[2]Díaz-Trigo et al. 2012 identify these two lines as FeXXV and FeXXVI K_β

corresponding to) 7 keV. The values in this column in EPN_CTI_0030.CCF are assumed equal to the weighted (by the statistical errors) mean of the values calibrated at the Si and Au instrumental edges. During the CCF validation process, the energy scale at the Fe line energies produced by the RDPHA will be compared with a larger sample of sources with narrow-band features at the Fe lines energies. The calibration will be changed accordingly, if required. Once again, we stress that such a change in the calibration *would not require a change in the SAS*, given the new tabular structure of the RDPHA_DERIV extension.

6 Test procedures and results

The results presented in the previous sections were obtained on 50 EPIC-pn Timing Mode exposures reduced with SASv13 (using the default withgaintiming=yes parameter in epchain). A further validation of this CCF will be performed once the RDPHA correction is implemented in SAS. Users are referred to the SAS Science Validation Reports (available at http://xmm.esac.esa.int/external/xmm_data_analysis/sas_validation/index.shtml) and to Guainazzi et al. (2013a) for updates on this topic.

7 Expected changes

The RDPHA is currently energy-independent. A study of its possible energy dependence is ongoing (cf. Sect. 5.2).

8 References

Dìaz-Trigo et al., 2012, A&A, 543, 50
Guainazzi M., 2013a, XMM-CCF-REL-299, (available at:
http:http://xmm2.esac.esa.int/docs/documents/CAL-SRN-0299-1-1.ps.gz)
Guainazzi M., 2013b, XMM-CAL-SRN-302, (available at:
http:http://xmm2.esac.esa.int/docs/documents/CAL-SRN-0302-1-0.pdf)
Guainazzi M., et al., 2008, XMM-SOC-CCF-REL-256, (available at:
http://xmm2.esac.esa.int/docs/documents/CAL-SRN-0256-1-0.ps.gz)
Guainazzi M., et al., 2013a, XMM-SOC-CAL-TN-0083 (available at:
http://xmm2.esac.esa.int/docs/documents/CAL-TN-0083.pdf)
Guainazzi M., et al., 2013b, XMM-CAL-SRN-304 (available at:
http:http://xmm2.esac.esa.int/docs/documents/CAL-SRN-0304-1-0.pdf)
Longinotti A. (ed.), et al., 2013, "XMM-Newton User's Handbook" (available at:
http://xmm.esac.esa.int/external/xmm_user_support/documentation/uhb/index.html)
Sala G., et al., 2008, A&A, 489, 1239
Smith M., 2004, XMM-SOC-CAL-TN-0050, (available at:
http://xmm2.esac.esa.int/docs/documents/CAL-TN-0050-1-0.ps.gz)